G. DANIEL DOCKERY and GERALD C. KONSTANZER

RECENT ADVANCES IN PREDICTION OF TROPOSPHERIC PROPAGATION USING THE PARABOLIC EQUATION

New algorithms implemented in the Electromagnetic Parabolic Equation (EMPE) propagation program have resulted in a capability to include a finitely conducting earth surface and most types of antenna patterns in propagation calculations. The antenna-pattern model has, in turn, made it possible to investigate monopulse radar performance in anomalous propagation conditions. Also, a simultaneous experimental effort has led to the development of a sophisticated range-interpolation scheme for refractive index variations and, ultimately, to validation of the EMPE program.

INTRODUCTION

Ideally, a model that would attempt accurate predictions of electromagnetic propagation in the troposphere should include the effects of transmitter/receiver geometry, frequency, polarization, antenna pattern, the earth's curvature, electrical properties of the earth's surface, surface roughness, and, of course, variations in the refractive index. Depending on the frequencies and atmospheric conditions of interest, it might be desirable to model atmospheric absorption and scattering as well. Although a model encompassing all of the foregoing effects has yet to be created, the Electromagnetic Parabolic Equation (EMPE) propagation program, under development at APL for the past several years, includes many of them.

EMPE was originally developed from an existing acoustic program by members of APL's Submarine Technology Department. The basic mathematical approach for EMPE was described by Ko, Sari, and Skura in a 1983 article[1] that also included a general introduction to the effects of anomalous propagation. At that time, EMPE could make propagation calculations that assumed a directed antenna beam above a smooth, perfectly conducting earth surface and that used specified refractive conditions that varied with both range and altitude; effects due to geometry and the earth's curvature were fully represented. In the past three years, algorithms have been added that model a finitely conducting earth surface and allow specification of any antenna pattern possessing symmetry or antisymmetry about the beam-pointing direction. An immediate consequence of this antenna-pattern model is that it is possible to represent monopulse radar operation in various propagation conditions.

Also during the last three years, several experiments involving atmospheric and propagation measurements have been conducted in an effort to validate the predictive capability of the EMPE program. A companion paper in this issue by Rowland and Babin describes the equipment and techniques used to make the atmospheric measurements; the experiments were devised and conducted by members of APL's Space Geophysics Group. To use the measured atmospheric data effectively in propagation calculations, it was necessary to develop a new algorithm that generates a physically reasonable scheme for the range evolution of refractive index structures. That algorithm has made it possible to use fully EMPE's ability to model propagation in complicated environments.

In this article, we briefly describe the finitely conducting boundary-condition and antenna-pattern algorithms and present some illustrative examples. We also discuss the method of performing monopulse calculations using the new antenna-pattern feature. Finally, after describing the atmospheric refractivity range-interpolation algorithm, we present some of the results of the experimental validation effort.

When describing refractive conditions in the troposphere, it is convenient to deal with a "modified refractivity" (M), usually presented as a profile versus altitude. M is related to the refractive index, n, as follows:

$$M = (n - 1 + z/a) \times 10^6 , \qquad (1)$$

in which z is the altitude and a is the earth's radius. Negative vertical gradients of M are associated with atmospheric ducts or trapping layers. Whether energy is ducted by a given "ducting" layer depends on the angle of arrival of the "rays" and on the thickness of the layer relative to the electromagnetic wavelength. All the refractivity conditions discussed below, whether hypothetical or measured, will be given as vertical profiles of M.

BACKGROUND

Although Fock described tropospheric propagation using parabolic equations as early as 1946,[2] the approach did not become attractive for complicated atmospheric conditions until 1973, when Tappert[3] successfully used the Fourier split-step algorithm to solve the parabolic wave

equation numerically. Tappert originally developed the technique to describe ionospheric propagation, but the algorithm has been most useful in describing the propagation of acoustic waves in the ocean,[4] which in many ways is directly analogous to electromagnetic propagation in the troposphere.

The vector wave equation describing propagation over a spherical earth can be reduced to a scalar parabolic equation, for either vertical or horizontal polarization, through a series of approximations that neglect the backscattered field and restrict the size of refractivity gradients that can be modeled.[1] The latter restriction excludes conditions that are rare in the troposphere. Further, the problem is easily translated to a pseudorectangular coordinate system, where the correction for the earth's curvature appears as a simple modification to the refractive index. The resulting parabolic equation is

$$\left\{\frac{\partial^2}{\partial z^2} + 2ik\,\frac{\partial}{\partial x} + k^2\left[n^2(x,z) - 1 + \frac{2z}{a}\right]\right\} \times u(x,z) = 0 , \quad (2)$$

where z is the altitude, x is the horizontal range, and k is a reference wave number typically taken to be $2\pi/\lambda$; λ is the electromagnetic wavelength in a vacuum. The quantity $u(x,z)$ varies slowly and is directly related to the tangential electric field (horizontal polarization) or the tangential magnetic field (vertical polarization). The boundary condition at the earth's surface is taken to be the impedance boundary condition derived by Senior[5] (among others):

$$\left.\frac{\partial u}{\partial z}\right|_{z=0} + \alpha u(x,0) = 0 , \quad (3)$$

where the quantity α is a function of the polarization and the absolute permittivity and conductivity of the surface.

Equations 2 and 3, combined with the radiation condition for $z \to \infty$, form the initial-value problem that is solved in the EMPE program. As will be described later, the initial condition at $x = 0$ is chosen to correspond to the desired antenna pattern. Numerical techniques that advance (or march) the solution in range may be applied to this initial-value formalism. In the EMPE program, the solution is advanced from one range to the next using the Fourier split-step algorithm.[3] This technique exploits the fact that the Fourier transform of Eq. 2 has a simple solution at $x + \delta x$ in terms of the solution at x, provided the refractive index can be considered locally constant in x and z. The split-step approach is advantageous in that it is easily implemented on a computer using a fast Fourier transform routine and it is stable and accurate for values of δx that are small relative to the scale of horizontal refractivity variations but large compared with a wavelength.

The appropriate Fourier transform is

$$U(x,p) = \int_{-\infty}^{\infty} U(x,z)e^{-ipz}\,dz , \quad (4)$$

where $p = k \sin\theta$ and θ is the angle from the horizontal. Then the split-step solution at $x + \delta x$ is

$$u(x + \delta x,z) = e^{i\frac{k}{2}(n^2 + \frac{2z}{a} - 1)\delta x} \times \int_{-\infty}^{\infty} U(x,p)\, e^{-i\frac{p^2\delta x}{2k}}\, e^{ipz}\,dp . \quad (5)$$

Thus, both forward and inverse transforms are required to advance one range step.

In general, the foregoing split-step solution requires full Fourier transforms, which in turn require knowledge of the field above and below $z = 0$. For a perfectly conducting surface, however, the boundary conditions are $u(x,0) = 0$ for horizontal polarization and $\partial u/\partial z = 0$ at $z = 0$ for vertical polarization; it follows from image theory that these boundary conditions are satisfied when u is odd or even, respectively, about $z = 0$. In such cases, the full Fourier transform can be replaced by a real sine or cosine transform, which involves knowledge of the field above the surface only and yields significant improvements in EMPE's computational efficiency.[6] New algorithms for EMPE, such as those described below, must apply image theory to preserve the advantages of using sine and/or cosine transforms.

FINITELY CONDUCTING EARTH'S SURFACE

When modeling microwave propagation over seawater, one can often make the approximation that the sea surface is perfectly conducting, particularly if the polarization is horizontal. Still, the finite conductivity of seawater does result in reduced amplitudes and additional phase shifts relative to the perfect-conduction values for the reflected fields; such effects are usually readily observable for vertically polarized waves. Furthermore, when considering propagation over regions of the earth where the conductivity is considerably lower than that of seawater, the electrical properties of the surface become important.

The effects due to polarization are contained entirely in the parameter defined as follows:[5]

$$\alpha = ik\left(\frac{\epsilon}{\epsilon_0} + i\,\frac{\sigma}{\omega\epsilon_0}\right)^{-1/2} \text{(vertical polarization)} \quad (6)$$

and

$$\alpha = ik\left(\frac{\epsilon}{\epsilon_0} + i\,\frac{\sigma}{\omega\epsilon_0}\right)^{1/2} \text{(horizontal polarization)}, \quad (7)$$

where ϵ_0 is the free-space permittivity and ϵ and σ are the absolute permittivity and conductivity of the surface, respectively. ω is the radian frequency of the electromagnetic waves.

To preserve the image-theory properties described in the preceding section, Eq. 3 is satisfied in EMPE using a linear combination of even and odd solutions,

$$u = Au_e + Bu_0 \ , \tag{8}$$

where A and B are complex combination constants. Substituting this expression into Eq. 3 and requiring the proper behavior for large and small values of α give the equations needed to solve for the real and imaginary parts of A and B. In this way, the even and odd solutions are combined to give the proper field at each range step in EMPE.

In the examples that follow, propagation over a smooth, finitely conducting sea is assumed. The values used for ϵ and σ correspond to a water temperature of 20°C and a salinity of 3.6%.[7] In particular, for 3 GHz, $\sigma = 7.02$ S/m and $\epsilon = 5.95 \times 10^{-10}$ F/m, and for 1 GHz, $\sigma = 5.43$ S/m and $\epsilon = 6.1 \times 10^{-10}$ F/m. Figure 1 presents the power relative to free space at an altitude of 305 m and a frequency of 3 GHz for vertical polarization. The antenna altitude is 31 m and a "standard atmosphere" refractive condition (i.e., a vertical gradient of 116.8 M/km) (Ref. 8) has been used. The EMPE results are compared with results generated by a method, described by Kerr,[8] that is applicable for the simple refractive conditions used here.

For a standard atmosphere and smooth sea, the primary effects of polarization and finite conductivity are observed in the null depths and peak heights in the interference region. Vertically polarized fields have a reflected amplitude smaller than that for horizontal polarization, resulting in less severe nulls over the same region. The variation in null depth with range, characteristic of vertical polarization at this frequency, is clearly evident in Fig. 1 and is in agreement with Kerr's model, which explicitly uses the proper reflection coefficients at the surface.

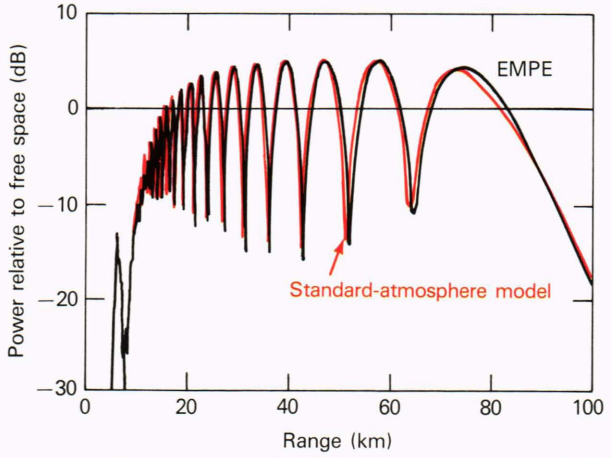

Figure 1—Results from EMPE and a simple standard-atmosphere model for a frequency of 3 GHz, an altitude of 305 m, and vertical polarization.

MODELING SPECIFIED ANTENNA PATTERNS

A familiar result of aperture antenna theory is that the radiated field is proportional to the Fourier transform of the field in the antenna aperture. Therefore, because Eq. 2 correctly accounts for diffraction from an aperture, Fourier transform theory can be used to provide an initial condition at $x = 0$ that will properly model the pattern shape, steered direction, and altitude of a specified antenna.

Calculation of an initial solution for EMPE begins with specification of a desired antenna pattern $F_d(p)$; the pattern may be measured data or data generated by an analytic expression. The aperture distribution is found by performing the inverse transform of $F_d(p)$,

$$f(z) = \frac{1}{2\pi} \int_{-\infty}^{\infty} F_d(p) e^{ipz} dp \ . \tag{9}$$

Using the Fourier shift theorem, a pattern is shifted to $p = p_{el}$, where $p_{el} = k \sin \theta_{el}$ and θ_{el} is the specified pointing angle, by introducing a linear phase factor in z-space:

$$\tilde{F}(p) \equiv F(p - p_{el}) = \int_{-\infty}^{\infty} f(z)\, e^{ip_{el}z}\, e^{-ipz} dz \ . \tag{10}$$

Similarly, the source is shifted to a specified altitude, z_s, by multiplying $\tilde{F}(p)$ by $\exp(-ipz_s)$. However, both even and odd initial solutions must be generated to satisfy the finite-conductivity boundary condition already described. Thus, the appropriate image sources must be generated for each case. For the even solution, one needs

$$U_e(0,p) = \tilde{F}(p)e^{-ipz_s} + \tilde{F}(-p)e^{ipz_s} \ , \tag{11}$$

and, in the odd case,

$$U_0(0,p) = \tilde{F}(p)e^{-ipz_s} - \tilde{F}(-p)e^{ipz_s} \ . \tag{12}$$

Equations 11 and 12 make up the initial conditions (in p-space) for the EMPE calculation. If the desired pattern is either symmetric or antisymmetric, all the expressions given above can be written in terms of real sine and/or cosine transforms, thus preserving the upper half-space formalism described previously.

Because the numerical solution in EMPE involves discrete Fourier transforms, there is a Nyquist sampling condition that must be satisfied. For a specified frequency and maximum problem altitude, the quantity corresponding to a "cutoff frequency" in the Nyquist criterion is the maximum problem angle, θ_{max}; that angle, measured from the horizontal, defines the region over which the EMPE solution is calculated. In the examples that follow, θ_{max} is approximately 13°, an angle at which the

EMPE-generated patterns will appear to be truncated. In practice, θ_{max} is chosen to be large enough to include all the angles of interest in the given problem.

Figure 2 presents normalized power versus altitude at ranges of 1.8, 5.5, and 9.3 km for a (sin p)/p pattern that has been steered to an angle of 2° above the horizon; the frequency is 1 GHz. The calculation assumed a flat earth and constant refractivity, which, when used with the antenna altitude of 1520 m, represent free-space conditions at close ranges.

Figures 3 and 4 compare EMPE-generated 40-dB Taylor and Bayliss patterns, respectively, with the desired patterns at a range of 7.5 km; once again, free-space conditions are approximated. To make the comparisons,

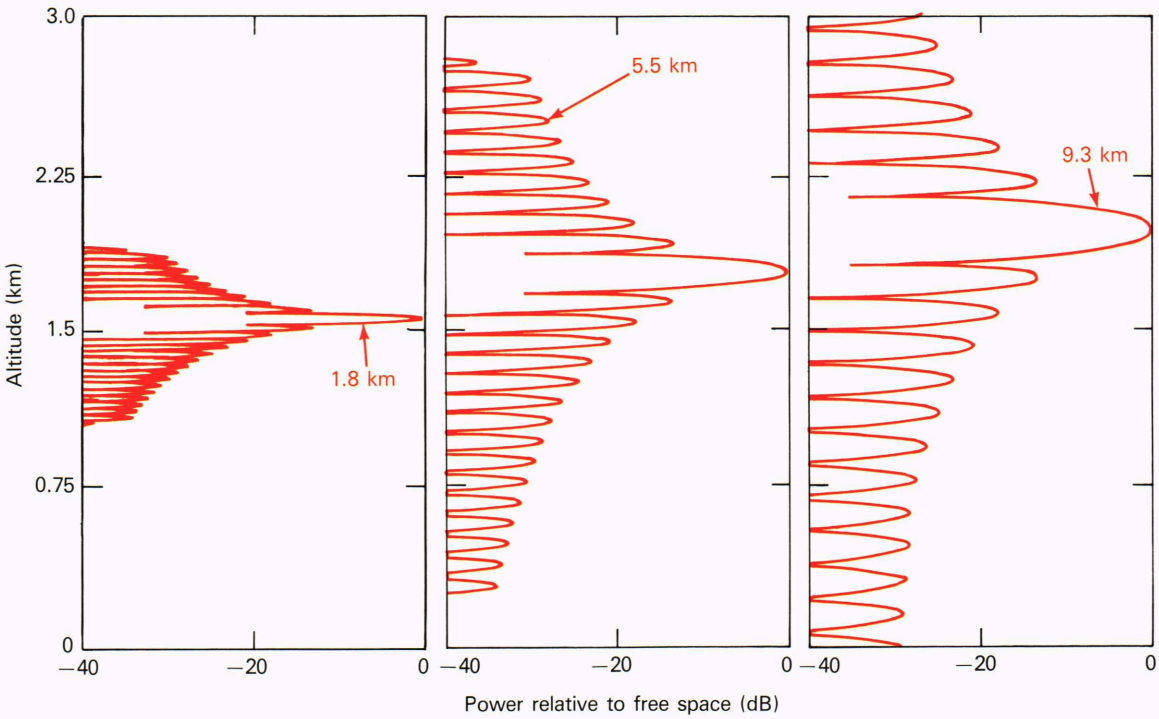

Figure 2—EMPE results for a (sin p)/p antenna pattern with an altitude of 1520 m and a pointing angle of 2°.

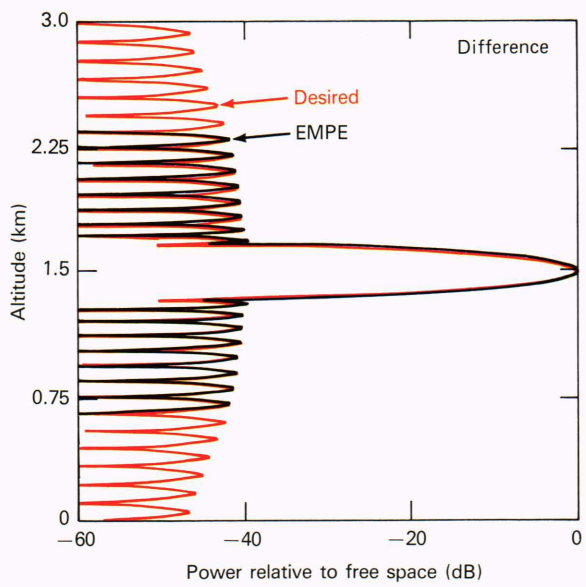

Figure 3—Comparison of specified and EMPE-generated Taylor patterns at a range of 7.5 km.

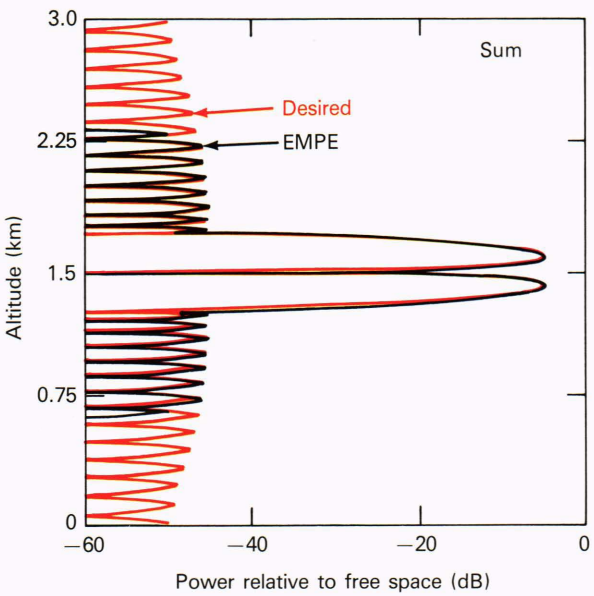

Figure 4—Comparison of specified and EMPE-generated Bayliss patterns at a range of 7.5 km.

it was necessary to plot the desired patterns in z-space. EMPE is demonstrated to match the desired patterns identically for $-\theta_{max} < \theta < \theta_{max}$. Similar agreement has been observed when using measured pattern data as the desired pattern.

MODELING MONOPULSE RADAR PERFORMANCE

In a monopulse radar system, difference and sum channels are typically used in both elevation and azimuth; the antenna patterns corresponding to the sum channels are symmetric, whereas the difference patterns are antisymmetric about the boresight direction. As a result of the central null in the difference pattern, the ratio of the difference and sum voltage patterns is a sensitive function of the arrival angle of the signal. In a monopulse radar, the ratio of the signals in the difference and sum channels can therefore be used in conjunction with a reference table to determine the monopulse angle error (angle from boresight) of the object being tracked. The patterns in Figs. 3 and 4 are typical of difference and sum receiving patterns, respectively. Although the power plot of the Bayliss pattern in Fig. 4 is symmetric, the voltage in the lower lobe is negative; this feature allows the system to determine which difference lobe the target is in by examining the phase of the difference signal relative to the sum signal.

In surface-based systems, an important aspect of monopulse radar operation is tracking performance at low elevation angles and in the presence of anomalous propagation conditions. In those situations, both the difference and sum patterns are often severely distorted; the distortion is usually worse for the difference pattern, since small elevation angles cause the lower difference lobe to illuminate the surface and/or to couple more strongly into surface ducts. Clearly, such conditions can profoundly affect the ratio of the difference and sum channel signals, which, in turn, affect the accuracy of target-angle estimates.

With its capability to model symmetric and antisymmetric antenna patterns, EMPE makes possible calculations using ideal or measured patterns corresponding to the difference and sum channels in a monopulse radar system. The procedure involves making separate propagation calculations, using appropriate difference and sum patterns, and then taking the ratio of the difference and sum results at each position (altitude and range) of interest. One possible monopulse implementation considers the real part of the complex error voltage ratio; that is,

$$V_{error} = Re\left[\frac{\psi_D}{\psi_S}\right] = \left|\frac{\psi_D}{\psi_S}\right| \cos(\phi_D - \phi_S) \ , \quad (13)$$

where ψ_D and ψ_S are the values of the field for the difference and sum pattern calculations, respectively. ϕ_D and ϕ_S are the phases of those fields.

The patterns used to generate Figs. 3 and 4 are used in the results presented here. A table of theoretical difference-to-sum error voltage ratio versus angle from boresight is generated using these patterns, and the table is then used to determine the apparent angle from boresight, given the error voltage ratio at any point in space.

In the following example, an antenna geometry and elevation angle are chosen along with a horizontal trajectory lying predominantly in the main beam of the sum pattern. The apparent monopulse angle error associated with each position along the trajectory is calculated using EMPE results for ψ_D and ψ_S, Eq. 13, and the table of voltage ratio versus angle error, mentioned above. The actual angle error, calculated from geometry, is also included for comparison.

In the results presented below, standard-atmosphere propagation conditions are assumed, and an altitude of 305 m is chosen for the trajectory. The antenna altitude is 30.5 m, and the beam is steered to a fixed elevation of 0.9°; the frequency is 1 GHz. Figure 5 shows the normalized power at 305 m for the two antenna patterns. The null in the difference pattern, somewhat corrupted by multipath interference, is visible at a range of 14 km. Note that the multipath nulls are substantially more severe for the difference pattern than for the sum pattern.

Figure 6 presents angle errors calculated from EMPE and from geometry. In the interference region, variations about the actual values result from the difference in multipath null depths between the two calculations. Beyond

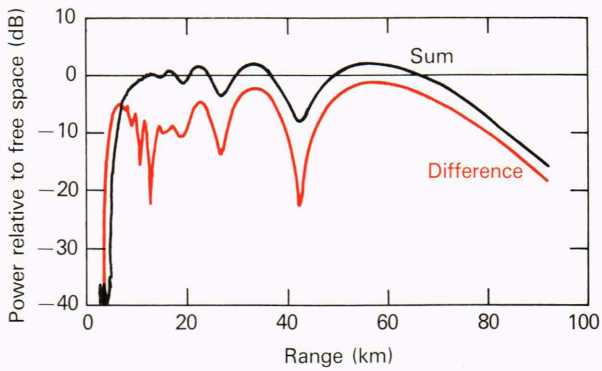

Figure 5—Results of standard-atmosphere EMPE calculations using the Taylor and Bayliss antenna patterns; the antenna altitude is 31 m and the frequency is 1 GHz.

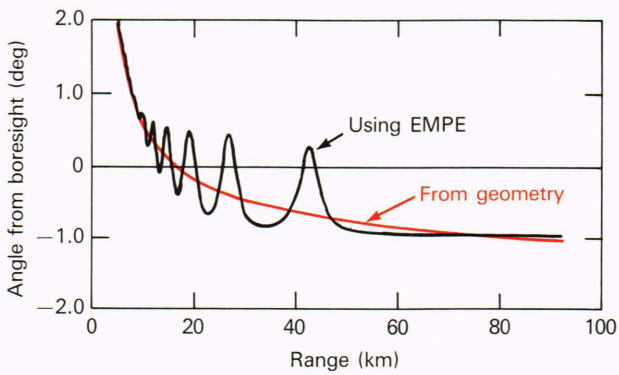

Figure 6—Correct and apparent monopulse angle errors for an object flying level at 305 m in standard atmospheric conditions.

about 55 km, the angle error becomes fixed (at approximately $-0.9°$) because the voltage ratio in the diffraction region is constant. These results are in complete agreement with monopulse calculations using other propagation models applicable in a standard atmosphere. The EMPE-based procedure described here can, however, be used to predict monopulse angle errors in most hypothetical or measured propagation environments.

REPRESENTING REFRACTIVITY VARIATIONS IN THE ATMOSPHERE

Refractivity layers in the lower atmosphere over the sea commonly result from temperature inversions or rapid changes in humidity. Boundaries between the layers are identified in refractivity profiles by changes in the vertical gradient. Layers large enough to affect propagation significantly at a particular frequency are considered large-scale profile structures. Any realistic model of the propagation environment must take into account that these structures can merge, separate, fade, or vary in the altitude over a range of a few kilometers.

The experiments described in the next section characterize the propagation environment by refractivity measurements collected aboard an instrumented helicopter along a trajectory describing a sawtooth pattern in range and altitude (Fig. 7). To facilitate use in EMPE, data collected along each ascent or descent are grouped into a high-resolution vertical profile of refractivity at one range location. In forming such profiles, altitude resolution is preserved at the cost of distorting the range resolution—a reasonable tradeoff because propagation in nearly horizontal directions is more significantly affected by altitude variations than by range variations of refractivity. The effect of altitude variations is especially significant in the presence of well-defined layers that commonly occur over the sea.

During a sawtooth flight involving atmospheric measurements, the helicopter will typically ascend or descend 300 m in a horizontal distance of 2 to 6 km. As a result, the profiles may be separated in range by several kilometers. The EMPE model, however, must have a refractivity profile specified at every calculation range, and the distance between the ranges may be a small fraction of a kilometer, depending on the frequency. It is necessary, therefore, to generate interpolated profiles at the ranges between measured profiles. Before such interpolation, it is important to correlate or match, in adjacent measured profiles, large-scale structures resulting from common layers. Matching allows layers to be tracked in range in a realistic manner.

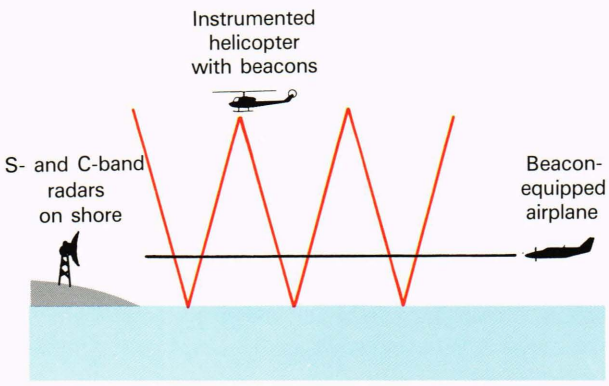

Figure 7—Arrangement for Wallops Island propagation experiments.

From its early stages of development, the EMPE program has had a built-in algorithm for performing such structure matching. When using complicated or strongly range-varying refractivity data, however, this algorithm may track refractivity layers erroneously. For that reason, a new matching routine, called LARRI (Large-scale Atmospheric Refractivity Range Interpolator), was developed for processing profiles before their use in EMPE.

LARRI has been designed to recognize 20 different types of refractivity structures, which have been organized into a hierarchy. LARRI begins by filtering out the measured small-scale structures that are not expected to persist from one calculation range to the next; at that point the profiles are also extrapolated up to a specified altitude. The algorithm then determines which of the remaining structures in the set of profiles are important, categorizes each important structure as one of the 20 types, and decides how these structures probably evolved in range. Structure matching is performed in each of the hierarchical categories, beginning with the most important; the decisions to match are based on the proximity and similarity of structures in adjacent profiles. In categories of lower importance, structures that cannot be matched are allowed to fade away between profiles. Finally, LARRI augments the profiles with additional points arranged so that structures are matched or faded according to the evolution scheme during the EMPE range-interpolation process.

Measured data collected during the October 1986 Wallops Island experiment, described in the next section, provide an excellent example of LARRI's operation. The data, presented in Fig. 8, exhibit severe range-dependence; a surface duct appears and disappears twice over the ranges shown. Figure 9 illustrates how LARRI filtered and matched the major structures of these profiles. The lines between profiles connect points that have been matched and will be interpolated in EMPE; to limit the line density, the lines shown correspond to half the points in the profiles. As will be shown in the next section, the agreement between EMPE/LARRI predictions using these data and the measured signal levels is very good. Executing EMPE using the unprocessed measured data proved impossible, because the original built-in algorithm was unable to identify a plausible range-evolution scheme for the data.

EXPERIMENTAL VALIDATION

The results presented in this article are from two EMPE validation experiments conducted at the NASA Wallops Island Flight Facility in August 1985 and October 1986. The purpose of the experiments was to record radar signal levels from aircraft flying a recorded trajectory through propagation environments where refractive characteristics were determined by helicopter

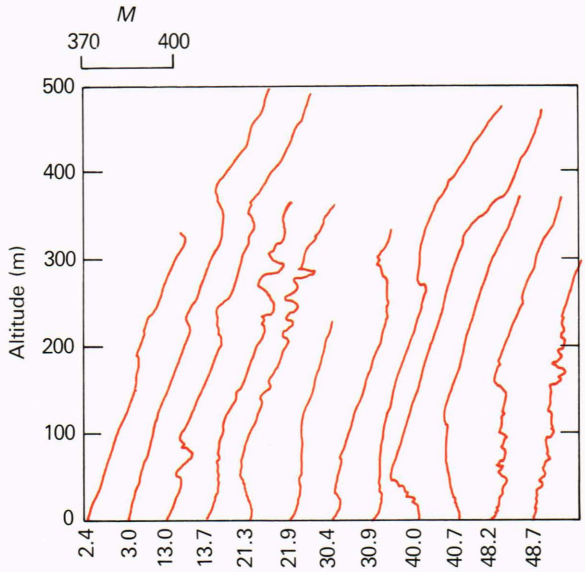

Figure 8—Refractivity profiles derived from unprocessed helicopter measurements taken on the morning of October 9, 1986. (Numbers across the bottom indicate range in kilometers; the range scale is not proportional. For each curve, *M* is measured by the projection of the curve onto the horizontal, using the scale at the top.)

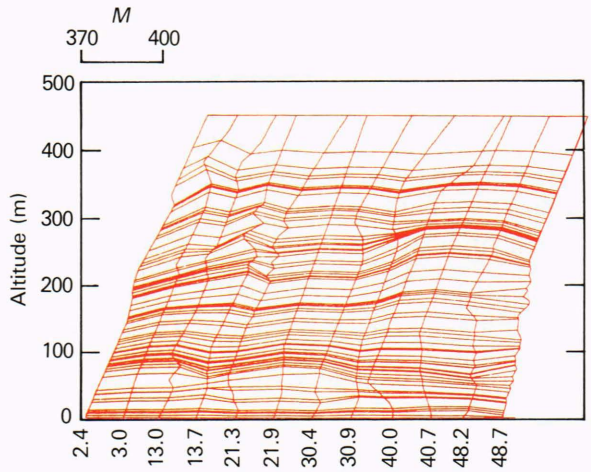

Figure 9—Smoothed and matched profiles with line segments connecting matched points. See Fig. 8 caption for explanation.

measurements. The refractivity data and parameters of the receiving radar system were used in EMPE to predict radar propagation in those environments. EMPE-calculated signal levels along the aircraft trajectory have been compared against the measured levels for validation.

The three Wallops Island radars used in the tests are the SPANDAR (Space Range Radar) research radar and the AN/FPQ-6 and AN/FPS-16 C-band tracking radars. SPANDAR is a high-power, narrow-beam radar that operates at S band. SPANDAR does not have a tracking capability, however, so it had to be slaved to one of the C-band tracking radars in order to be pointed at the target of interest. Figure 7 is a general schematic representation of the experimental arrangement. Figure 10 indicates the location of Wallops Island and SPANDAR on Virginia's Eastern Shore; a typical radial flight path is also shown.

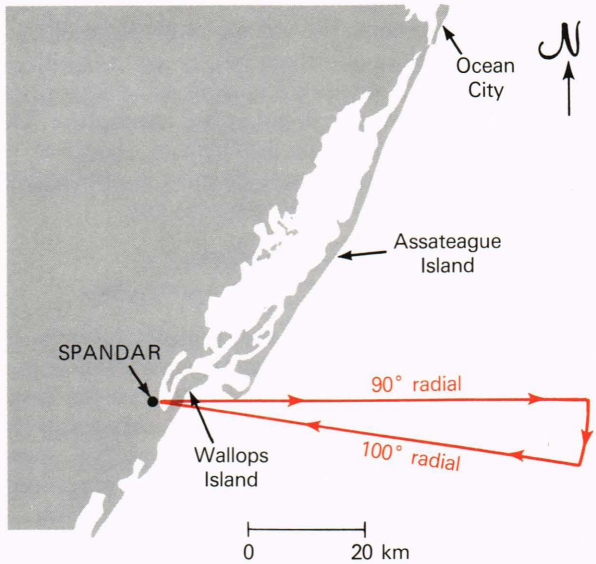

Figure 10—Location of Wallops Island experiments with a typical flight path of helicopter and/or airplane.

In both experiments, signal levels from S- and C-band aircraft transponders were recorded at the SPANDAR and tracking radar facilities. Since the radar data were recorded as received power versus range, EMPE was used to calculate path loss—which includes the full range dependence—rather than power relative to free space. Relative normalization of the predicted and recorded signal levels was accomplished by requiring the two signals to agree at the closest coincident range.

The first experiment was conducted from August 12 to 16, 1985, using a beacon-equipped Bell Jet Ranger helicopter, which flew over water, along specified radials from SPANDAR, to a distance of 75 km. Between flights, SPANDAR scanned the environment for long-range surface clutter and atmospheric returns indicative of ducting. Figure 11 presents photographs of two typical SPANDAR-generated PPI (Plan Position Indicator) scans separated by 1 h 23 min; the scans were performed during a different test conducted on April 12, 1985. The photographs demonstrate that the environment can change significantly in a short time. Information from PPI scans was used to direct the helicopter to areas that appeared to have interesting propagation conditions.

Figure 12 shows refractivity profiles derived from helicopter measurements taken the afternoon of August 15. The first, very different from the others, is located at the land–sea boundary, where conditions often vary rapidly in range. Because the down-range profiles indicate the presence of a 100-m surface duct, which is repeatable over a distance of 24 km, the profile at 37.8 km was replicated at 9 km to moderate the effect of the unusual (and probably local) profile at 3.7 km.

Figures 13 and 14 compare EMPE-generated and observed signal levels for S and C bands, respectively. The

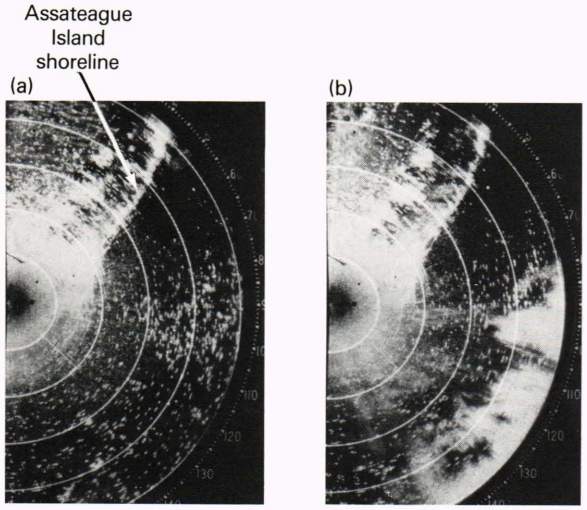

Figure 11—PPI scans performed by SPANDAR on April 12, 1985. (a) 13:57:23 local time. (b) 15:20:13 local time.

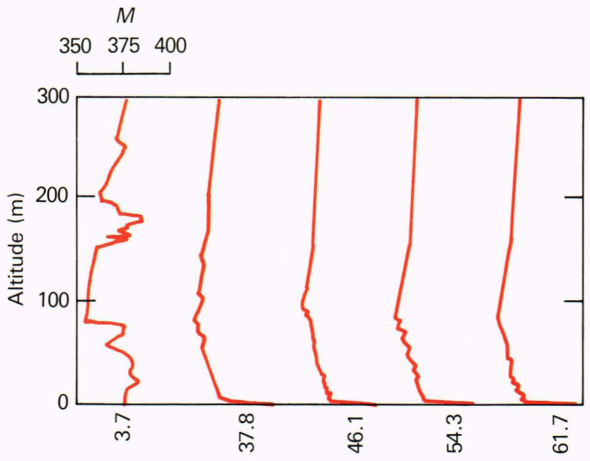

Figure 12—Refractivity profiles for the afternoon of August 15, 1985. (Numbers across the bottom indicate range in kilometers. For each curve, *M* is measured by the projection of the curve onto the horizontal, using the scale at the top.)

ranges at which the received power is higher correspond to the periods when the helicopter was low and inside the duct; the received power decreased when the helicopter climbed into the "fade" region above the duct and below the horizon. For ranges beyond 37 km, the helicopter was below the horizon throughout its sawtooth cycle. As expected, the fades are more severe for the C band because the higher frequency radiation is more effectively trapped by the duct. The regions where no EMPE results are given correspond to ranges at which the helicopter was not recording altimeter data. Regions where measured data are lacking correspond to periods when the C-band radar did not have a good track of the aircraft; bad track data usually resulted from low C-band signal levels.

The second Wallops Island experiment was conducted from October 8 to 11, 1986, using a Piper twin-engined airplane as the target aircraft from which transponder signals were received and recorded. The airplane flew level flights at an altitude of 31 m, along the same radial as the helicopter, which was collecting atmospheric data in the usual manner.

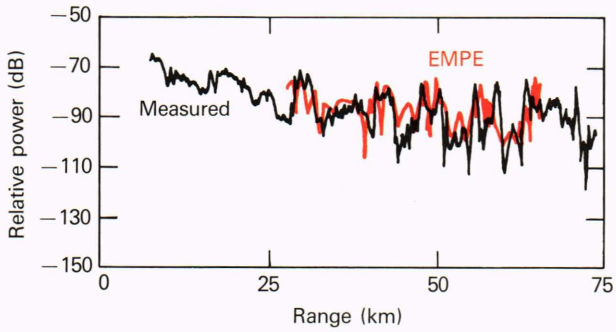

Figure 13—EMPE-generated and measured S-band signal levels for helicopter transponder during a sawtooth flight, August 15, 1985.

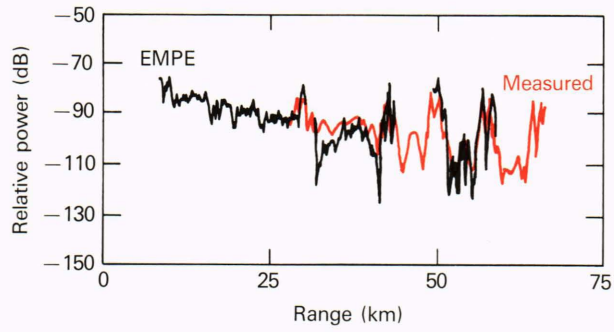

Figure 14—EMPE-generated and measured C-band signal levels for helicopter transponder during a sawtooth flight, August 15, 1985.

The profiles in Fig. 8 were collected on the morning of October 9; these strongly range- and altitude-dependent profiles were processed by LARRI for use in EMPE. Because the airplane was flying much faster than the helicopter, it made three radial passes while collecting the corresponding refractivity data; Fig. 15 compares calculated and measured C-band signal levels for the three flights. The largest discrepancy is that the measured data do not exhibit the predicted 10-dB multipath null at approximately 22 km; that multipath interference probably has been destroyed by the random effects mentioned above. For the most part, however, the mean signal levels are successfully predicted by EMPE.

Although the experimental results described here represent only a portion of the work that has been done in the effort to validate EMPE, they are representative of the performance level regularly exhibited by EMPE. Thus far, all cases examined have resulted in good agreement between EMPE predictions and measurements.

CONCLUSIONS

The EMPE propagation program has been continuously refined and upgraded since it was first developed several years ago. In its current form, EMPE has demon-

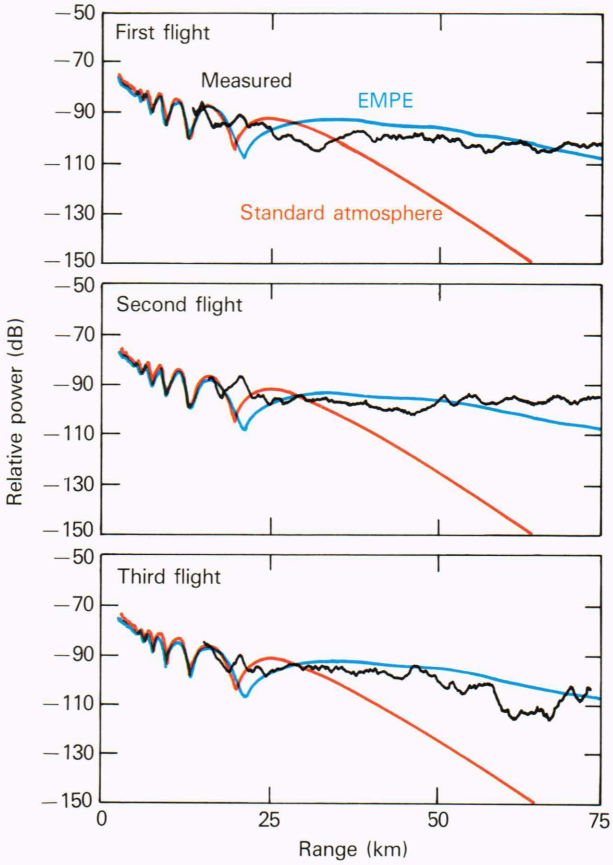

Figure 15—EMPE-generated and measured C-band signal levels for a Piper airplane transponder during three level flights, October 9, 1986.

strated the ability to predict accurately the distribution of electromagnetic energy in the troposphere in complicated refractivity environments that are difficult or impossible to represent using other propagation models.

In pursuit of the continued improvement of EMPE, considerable effort is being expended on the development of rough-surface and sea-swell models. The effects on propagation of small-scale and random refractivity fluctuations are also being investigated to determine the resolution of atmospheric measurement required for effective propagation prediction. Incorporation of random surface and atmospheric effects would make it possible for EMPE to predict the rapid fluctuations that are often observed in measured data and to include tropospheric scattering effects.

REFERENCES

[1] H. W. Ko, J. W. Sari, and J. P. Skura, "Anomalous Microwave Propagation Through Atmospheric Ducts," *Johns Hopkins APL Tech. Dig.* **4**, 12–26 (1983).

[2] V. A. Fock, "Solution of the Problem of Propagation of Electromagnetic Waves Along the Earth's Surface by Method of Parabolic Equations," *J. Phys. USSR* **10**, 13–35 (1946).

[3] F. R. DiNapoli and R. L. Deavenport, "Numerical Methods of Underwater Acoustic Propagation," in *Ocean Acoustics*, J. A. DeSanto, ed., Springer-Verlag, pp. 135–137 (1977).

[4] F. D. Tappert, "The Parabolic Approximation Method," in *Wave Propagation and Underwater Acoustics*, J. B. Keller and J. S. Papadakis, eds., Springer-Verlag, pp. 224–286 (1977).

[5] T. B. A. Senior, "Impedance Boundary Conditions for Imperfectly Conducting Surfaces," *Applied Sci. Res.*, Sec. B, **8**, 418–436 (1960).

[6] J. W. Cooley, P. A. W. Lewis, and P. D. Welch, "Fast Fourier Transform Algorithm: Programming Considerations in the Calculation of Sine, Cosine, and Laplace Transforms," *J. Sound Vib.* **12**, 315–337 (1970).

[7] J. A. Saxton and J. A. Lane, "Electrical Properties of Sea Water," *Wireless Eng.* **29**, 269–275 (Oct 1952).

[8] D. E. Kerr, *Propagation of Short Radio Waves*, McGraw-Hill, New York (1951).

ACKNOWLEDGMENTS—Many people at APL have contributed to the development and validation of the EMPE propagation model. Much of the credit is due to the efforts of H. Ko, J. W. Sari, J. P. Skura, and R. I. Joseph, who originally applied the parabolic equation/Fourier split-step approach to tropospheric propagation problems and who have continued to contribute to the advancement of EMPE. Credit goes to P. Vandyke for the algorithm used to implement an impedance boundary condition. Also, in the theoretical aspects of the propagation model, discussions with M. E. Thomas and J. R. Kuttler have proven very valuable.

The propagation experiments used in the validation of EMPE were in large part conducted by J. R. Rowland and S. M. Babin under the supervision of J. Goldhirsh. Mr. Rowland has also contributed heavily to the understanding of the various atmospheric processes observed during this effort.

THE AUTHORS

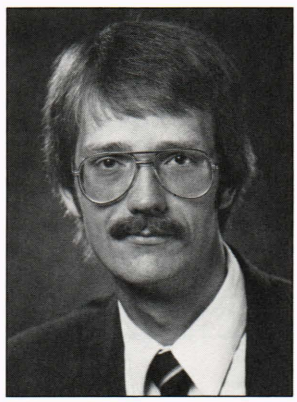

G. DANIEL DOCKERY received a B.S. degree in physics in 1979 and an M.S. degree in electrical engineering in 1983 from Virginia Polytechnic Institute and State University. During 1980–81, he was involved in the design and testing of high-power, millimeter-wave devices at Harry Diamond Laboratories in Adelphi, Md. As a research assistant at VPI&SU, he was engaged in modeling the propagation of ultrasonic waves in fluids.

Mr. Dockery came to APL in 1983 and joined the Combat Systems Development Group in the Fleet Systems Department. He has been involved in planar array antenna design and, more recently, in the modeling and measurement of electromagnetic wave propagation in the troposphere. This work has led him to investigations of the performance of specific radar systems in anomalous propagation environments.

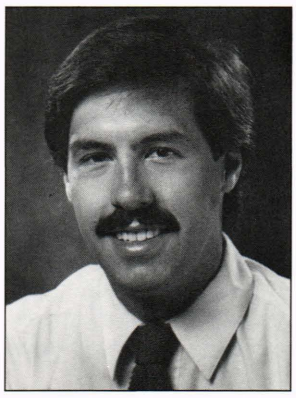

GERALD C. KONSTANZER was born in 1961 in Philadelphia. He studied biomedical and electrical engineering at Temple University and in 1983 received his B.S.E.E.T. In 1985, he received his M.S.E.E. from Drexel University. As a graduate research assistant, Mr. Konstanzer coauthored several conference papers on the minimal-time maneuver detection problem in conjunction with the Naval Air Development Center. He joined the Radar Systems Analysis Section of APL's Fleet Systems Department in 1985. His current areas of research include the characterization of anomalous propagation environments, the study of superresolution techniques for low-elevation target/multipath discrimination, and the investigation of pulse-Doppler clutter filtering methods.